



**HAL**  
open science

## Sealing of concrete confining structures of French nuclear reactors

Yan Pei, Shucaï Li, Franck Agostini, Frédéric Skoczylas, Benoît Masson

► **To cite this version:**

Yan Pei, Shucaï Li, Franck Agostini, Frédéric Skoczylas, Benoît Masson. Sealing of concrete confining structures of French nuclear reactors. *Engineering Structures*, 2019, 197, pp.109283. 10.1016/j.engstruct.2019.109283 . hal-02894316

**HAL Id: hal-02894316**

**<https://hal.science/hal-02894316>**

Submitted on 25 Oct 2021

**HAL** is a multi-disciplinary open access archive for the deposit and dissemination of scientific research documents, whether they are published or not. The documents may come from teaching and research institutions in France or abroad, or from public or private research centers.

L'archive ouverte pluridisciplinaire **HAL**, est destinée au dépôt et à la diffusion de documents scientifiques de niveau recherche, publiés ou non, émanant des établissements d'enseignement et de recherche français ou étrangers, des laboratoires publics ou privés.



Distributed under a Creative Commons Attribution - NonCommercial 4.0 International License

# 1 Sealing of concrete confining structures of French nuclear reactors

2 Yan Pei <sup>a,b</sup>, Shucaï Li <sup>a</sup>, Franck Agostini <sup>b,\*</sup>, Frédéric Skoczylas <sup>b</sup> and Benoît Masson <sup>c</sup>.

3

4 <sup>a</sup> Geotechnical and Structural Engineering Research Center, Shandong University, 250061,  
5 Jinan, China.

6 <sup>b</sup> Univ. Lille, CNRS, Centrale Lille, FRE 2016 – LaMcube – Laboratoire de mécanique  
7 multiphysique et multiéchelle, F-59000, Lille, France

8 <sup>c</sup> Electricité de France (EDF-SEPTEN), SEPTEN - Division GS - Groupe EN 69628  
9 Villeurbanne Cedex, France.

10 \* Corresponding author.

11 email address: peiyan@sdu.edu.cn, lishucaï@sdu.edu.cn, franck.agostini@centralelille.fr,  
12 frederic.skoczylas@centralelille.fr, benoit.masson@edf.fr

13

14

15 **ABSTRACT**

16

17 France has a total of 58 nuclear reactors, which produce 75% of its electricity. The second-  
18 generation reactors are protected by two concentric concrete envelopes, which are separated  
19 by an annular space. Every ten years, leakage tests are performed, by inflating the  
20 confinement structure with pressurized dry air. The confining structures of several second-  
21 generation reactors are now close to their allowed leakage limit. As a consequence, several

22 different approaches are currently being studied in order to improve their airtightness. A  
23 dedicated wall has been especially designed, by our laboratory, to simulate the leakage tests  
24 as they occur in the real in-situ confining structures. The main goal of this “apparatus” was to  
25 test different possibilities to recover a large part of the envelope tightness: application of  
26 coatings or water re-saturation of the concrete with spraying. The measured airtightness and  
27 bond strength (between the wall and coating) of two concrete prototypes revealed these to be  
28 unsatisfactory. In parallel, the spraying method allowed a high proportion of the concrete's  
29 gas tightness to be recovered. The present study provides a detailed description of the design  
30 of the prototype test wall and the results of preliminary tests, including those obtained with  
31 the "water spraying technique".

32

## 33 1 INTRODUCTION

34 France has 58 nuclear reactors, supplying the country with approximately 75% of its  
35 electricity requirements. The average age of these reactors is around 30 years, and EDF  
36 ('Electricité de France', operator of the nuclear reactors) is considering the extension of their  
37 useful life for several more decades. In the framework of its safety calculations for the  
38 reactors' concrete containment structures, EDF is required to carry out ten-year dry air  
39 pressurization tests – up to a relative pressure of 4 bars - and to determine the corresponding  
40 leakage rates. These tests, accompanied by the identification of flow mechanisms in a porous  
41 matrix or in a cracked (or pre-cracked) zone of concrete, are required to demonstrate that  
42 under accidental conditions, the global leakage will not exceed a regulatory upper safety limit.  
43 Recent tests have shown that some second-generation containment envelopes (double  
44 containment structures) are in need of refurbishment to improve their gas-tightness (**Figure**

45 1), and various reinforcement scenarios requiring modifications to the outer surface of the  
46 internal containment envelope are currently being studied. The most likely approach,  
47 involving the construction of a new concrete sarcophagus around the internal envelope, would  
48 nevertheless be a lengthy and expensive solution. Before initiating any real (in-situ) design  
49 work, two physical aspects need to be studied in detail: the improvement in airtightness, and  
50 the bond strength of the coating applied to the confinement wall. The strength and durability  
51 of the coating's bond is undoubtedly the most critical aspect, since the envelope's airtightness  
52 can certainly be improved through the choice of efficient coating materials (polymers, ultra  
53 high performance fibre-reinforced concrete or UHPFC, etc.). Our laboratory (LamCube) was  
54 given the task of validating (or rejecting) various potential solutions, and a dedicated wall was  
55 designed and built for the purposes of leakage test simulations. The gas tightness and bond  
56 strength (between the wall and coating) of two ultra-high-performance, fibre-reinforced  
57 concrete solutions were evaluated. Few tests have been already performed, mainly in France  
58 with the Maeva mock-up [15], which is like a reproduction, at a lower scale, of a real  
59 confining structure. Despite its smaller scale, it does not allow to test, in a reasonable period  
60 of time, different coating solutions. It is why the wall has been designed and its originality lies  
61 in the fact that it is able to reproduce a pressurization in-situ test. To our knowledge such a  
62 mock-up is unique in the world.

63 Our team has worked on gas relative permeability measurements on rocks and cementitious  
64 materials for nearly 20 years. Numerous tests and measurements have provided considerable  
65 insight into the behaviour of these materials, allowing the following crucial question to be  
66 answered: why do concrete structures becoming increasingly permeable to gas over time?  
67 Two main causes have been identified:

- 68       • The first and clearly most important of these is the concrete drying process. Many  
69       published results [1,2,3] have shown that the effective gas permeability i.e. gas  
70       permeability measured on a partially water saturated material, can increase by two or  
71       three orders of magnitude, when the material varies from the (almost) fully saturated  
72       state to the dry state.
- 73       • The second factor is cracking and/or microcracking. Many different experiments have  
74       shown that the gas permeability of a concrete structure is very sensitive to this  
75       phenomenon [4,5]. The causes of cracking are multiple: shrinkage due to drying,  
76       mechanical and thermal effects, interface degradations (concrete joints, contact zones  
77       between the concrete and other materials such as reinforcement bars, prestressing  
78       cables, ... ).

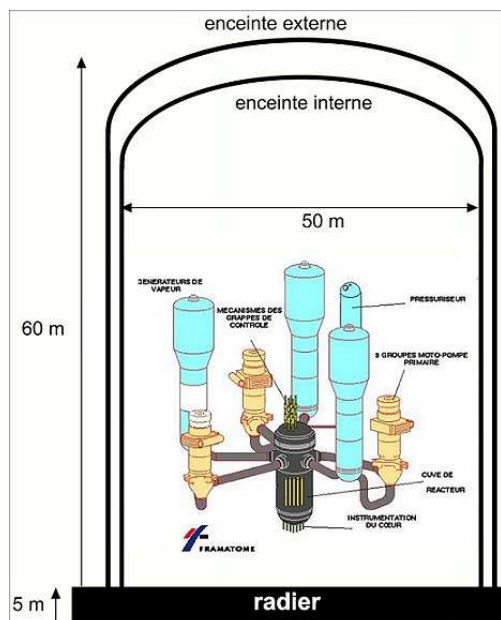
79

80   One potential solution, designed to decrease the permeability of the concrete envelope,  
81   involves the notion of mechanically closing the cracks. This is based on the use of an  
82   additional means of applying external prestress to the concrete, in order to close the existing  
83   cracks and thus reduce their permeability. However the experiments reported by Chen et al.  
84   and Wang et al. [4,5] have shown that even when they are mechanically closed, macro-cracks  
85   lead to concrete permeability that is much higher than that observed in the same intact  
86   material. Moreover, adding a new pre-stressing disposal cannot ensure that the pre-existing  
87   cracks will be closed. Hence, since the complexity of this type of structure does not allow  
88   reliable simulations to be performed, this approach was abandoned.

89

90 In parallel, our laboratory has worked on a different approach, which consists in simply  
91 spraying water onto dry, cracked concrete. The aim of this "simple" technique is to recover  
92 most of the concrete's gas tightness (relative permeability), through an increase in its water  
93 saturation [6,7], moreover the resulting imbibition would lead to concrete swelling and crack  
94 closure. The present study focuses on the aforementioned topics, i.e. the design of a prototype  
95 concrete wall, the first tests performed with UHPFC coatings and the first results obtained  
96 using the "water spraying technique". On a physical point of view, these tightening solutions  
97 cannot be analysed by the same methodology. The coating solution mainly requires the  
98 bonding strength to be evaluated whereas the spraying technics is linked to gas permeability  
99 decrease of concrete due to its re-saturation with liquid water. Hence this paper has been  
100 divided into two parts. The first one focuses on the description of the wall design and the  
101 UHPFC coating performances (on a mechanical point of view). The second part is dedicated  
102 to the spraying technics and to the results obtained on small structures and on the wall.

103



104

105 *Figure 1: Schematic view of a second generation nuclear power plant*

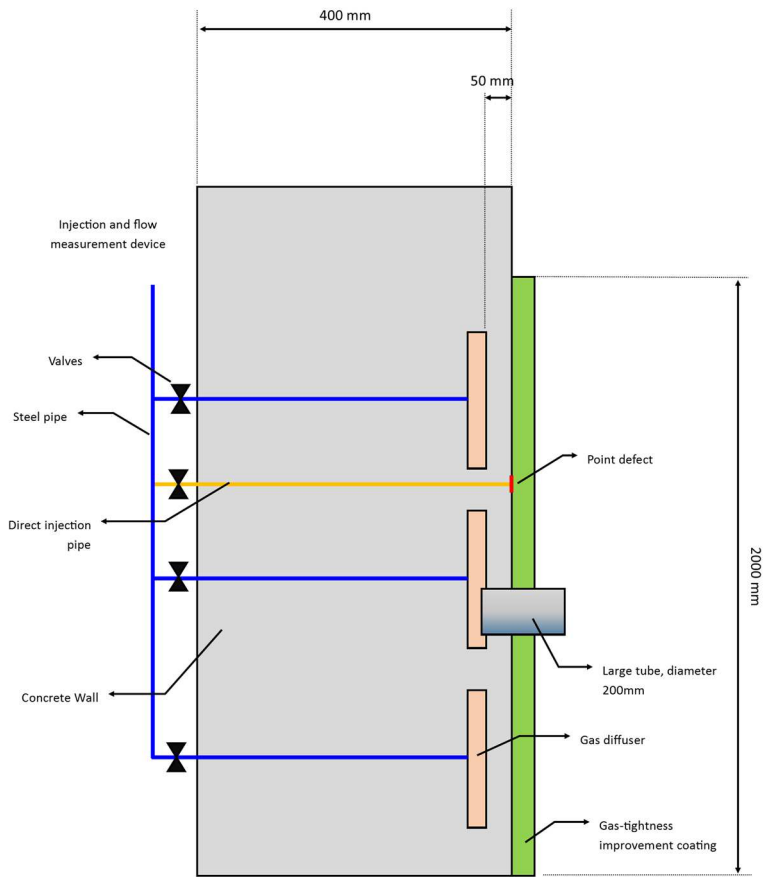
106        **2 Part 1: DESIGN OF THE WALL – COATING PREPARATION and**  
107            **TESTING**

108        **2.1 Design of the wall**

109        The test wall was designed to simulate the behaviour of concrete inside a closed confinement  
110        structure, under internally pressurized air. Several technical specifications were imposed:  
111        representative scale, ability to reproduce a diffuse flow of gas, similar to real in-situ  
112        conditions, and the ability to receive layers of coatings made from concrete, polymers or geo-  
113        polymers. Small concrete slab samples were already tested for which the gas pressure is  
114        applied to the coating at a single point, via a small interface defect. The conditions  
115        encountered with this type of device are quite different to those encountered in a real  
116        confinement structure, in which the entire interface is subjected to the gas pressure. For this  
117        reason, it was decided to build a large, dedicated wall: 6.90 m wide, 2.30 m high and 40 cm  
118        thick. The wall was divided into three identical, but independent concrete slabs, allowing  
119        three different approaches to the gas-tight sealing of concrete to be tested. Six gas diffusers  
120        and one direct injection point were installed 5 cm below the outer surface of each of these  
121        three slabs (**Figure 2** and **Figure 3**), and the gas pressure (or flow rate) was controlled  
122        independently within each diffuser. The gas pressure of each diffuser can be varied up to  
123        8 bars at the wall/coating interface, which is the maximum value specified by EDF. Although  
124        the rear side of the diffusers was designed to be gas-tight, a small level of leakage occurred at  
125        the rear the wall. Nevertheless, as the main requirement is to stabilise the gas pressure at the  
126        wall/coating interface, such small leaks are not particularly problematic; the gas pressure is  
127        measured at the interface between the wall and the coating through the gas injection points  
128        (shown in red in **Figure 2**). Strong steel reinforcement was used in order to avoid any risk of  
129        delamination (see **Figure 3**), especially during the coating test, for which the surface is almost

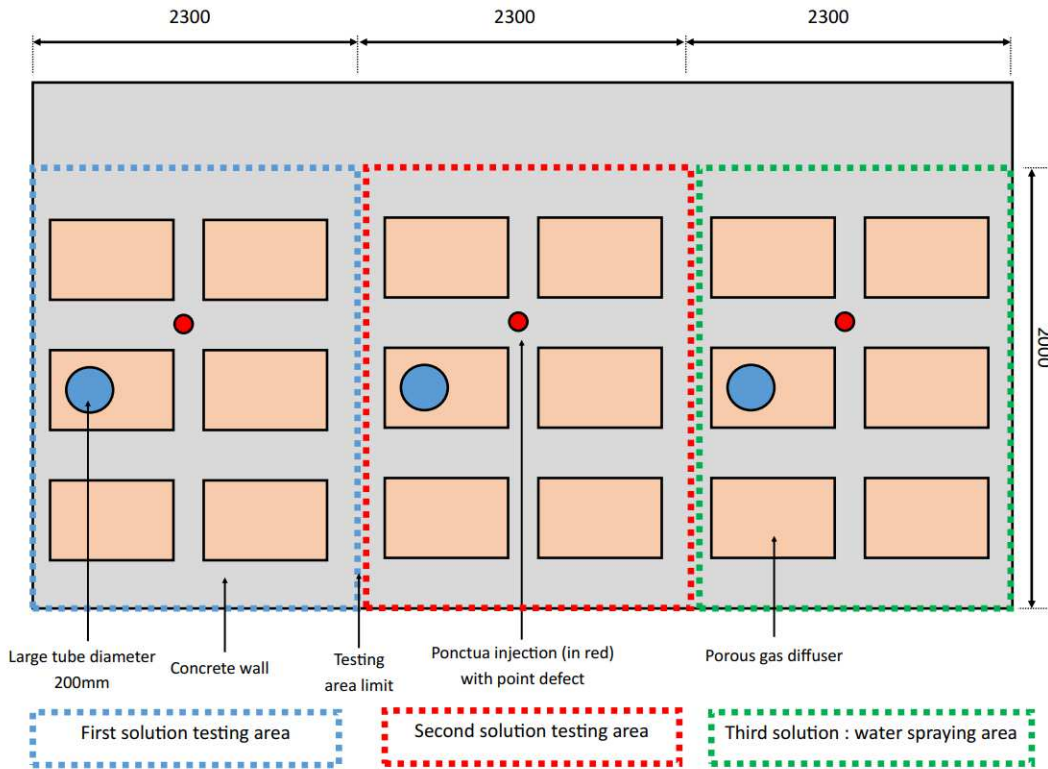
130 airtight. The test wall was built according to our calculations and specifications by the  
131 NORPAC company (owned by the Bouygues Group). The concrete used for this structure was  
132 self compacting, (consistency class SF2), with a high W/C ratio (0.65) in order to ensure a  
133 substantial level of porosity It is a C25/30 concrete made with CEM II/A-LL 42.5 R CE CP2  
134 NF cement. This is the sole important characteristic for this material as this can ensure a  
135 relatively quick drying leading to cracking occurrence. Laboratory measurements indicated:  
136 15.2% mean water porosity and  $2.5 \cdot 10^{-17} \text{ m}^2$  mean dry gas permeability. *The technics used to*  
137 *measure these properties are quite usual in our laboratory and can be found in [3].* The wall  
138 was then covered with a canvas sheet, and hot air was blown over its front surface for almost  
139 18 months. The aim of this operation was to obtain a dried concrete layer in front of the  
140 diffusor, and to promote cracking due to desiccation [8], thus ensuring its high gas  
141 permeability. On the other hand, the concrete behind the diffuser (with a thickness of 30 cm)  
142 was intended to remain almost fully saturated, i.e. to ensure that this portion of the concrete  
143 wall had a low gas permeability. A complete map of the wall's major leaks was produced,  
144 through the use of soapy water and the measurement, at each diffuser, of the gas flow rate  
145 induced by an injection pressure of either 2 or 4 bars (see Figure 22)

146



147

148 a)



149

150 b)

151 *Figure 2: Schematic cross-sectional view (a) and front view of the wall, designed to have three independent test sections. The*

152 *red points (injection points) are used to measure the gas pressure at the interface.*

153



154

155 *Figure 3: Steel reinforcement, large tube, diffusers and rear side of the wall, showing the injection tubes and valves.*

## 156 2.2 Coating preparations

157 Two different procedures were tested, both of which are based on the use of ultra-high-  
158 performance fibred concrete (UHPFC). Two of the concrete slabs were used: in a preliminary  
159 step, these were sand-blasted in order to optimize the coatings' adhesion to the wall. This type  
160 of substrate preparation appears to be the most efficient to obtain the maximum bond strength  
161 [11-12].

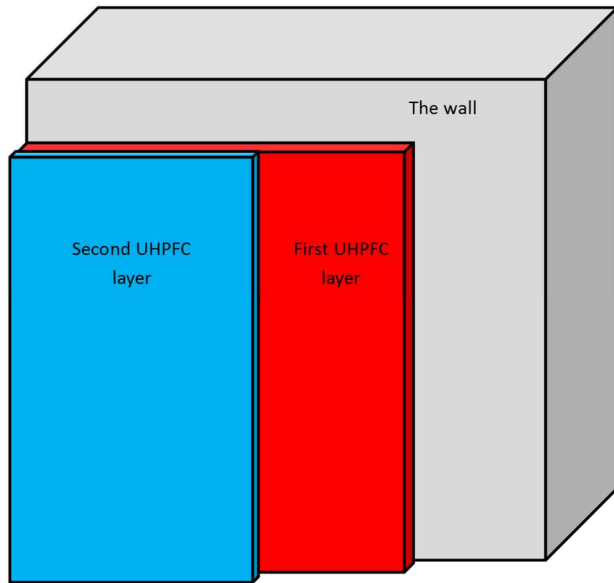
162 The first of these involved the application of two UHPFC layers, each having a thickness of  
163 3 cm. These layers were applied directly to the wall in two successive steps (**Figure 4** and  
164 **Figure 6**).

165 The second procedure made use of (3 cm thick) precast hexagonal shells, which were attached  
166 to the wall by means of special screws. The gap between the shells and the wall was then  
167 filled with UHPFC (**Figure 5** and **Figure 6**). It was decided to perform gas-tightness

168 measurements and strength evaluations of these two methods, one month after their  
 169 preparation. It must be underlined here that all the layers and the shells were composed with  
 170 the same UHPFC. This concrete was designed, prepared and applied on the wall by its  
 171 producer. Its composition and the way it is prepared are confidential and cannot be detailed in  
 172 this paper. Typical compositions for this kind of concretes can be found in the literature.  
 173 Spasojevic [16] has collected compositions datas of several UHPFC which are summarized in  
 174 Table 1. Furthermore, the UHPFC concrete used in this study presents a porosity lower than  
 175 10% and a gas permeability less than  $10^{-19}$  m<sup>2</sup>.

Component	UHPC matrix composition [16] kg/m <sup>3</sup>
Portland cement	700 – 1000
Coarse aggregate	0 - 200
Fine aggregate, Sand	1000 – 2000
Silica fume	200 – 300
Superplasticizers	10 - 40
Fibres	>150
Water	110 - 200

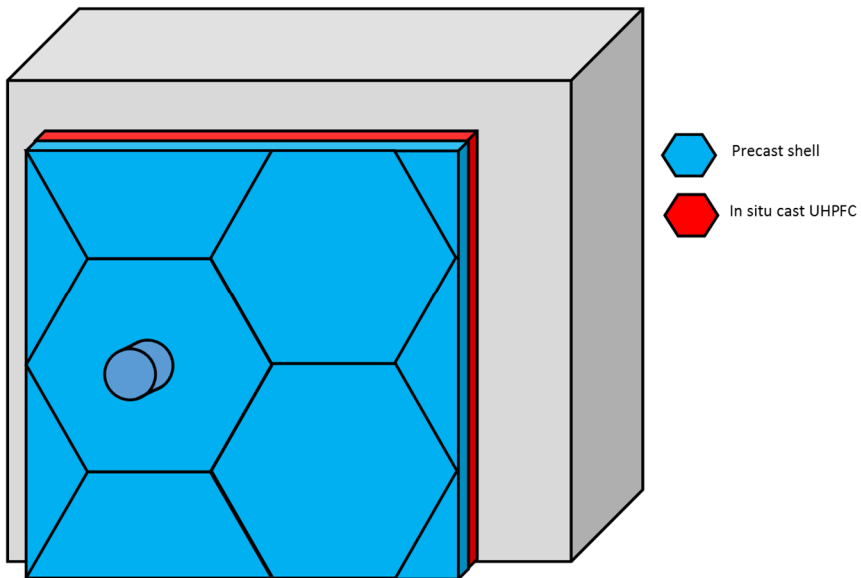
176 *Table 1: examples of composition of UHPC concrete from [16].*



177

178 *Figure 4: First solution. Layers applied directly to the wall*

179



180

181 *Figure 5: Second solution. Precast shells screwed onto the wall and sealed with UHPFC.*



182

183 *Figure 6: Pictures of the wall showing coating work and the two different solutions.*

### 184 2.3 Coating tests

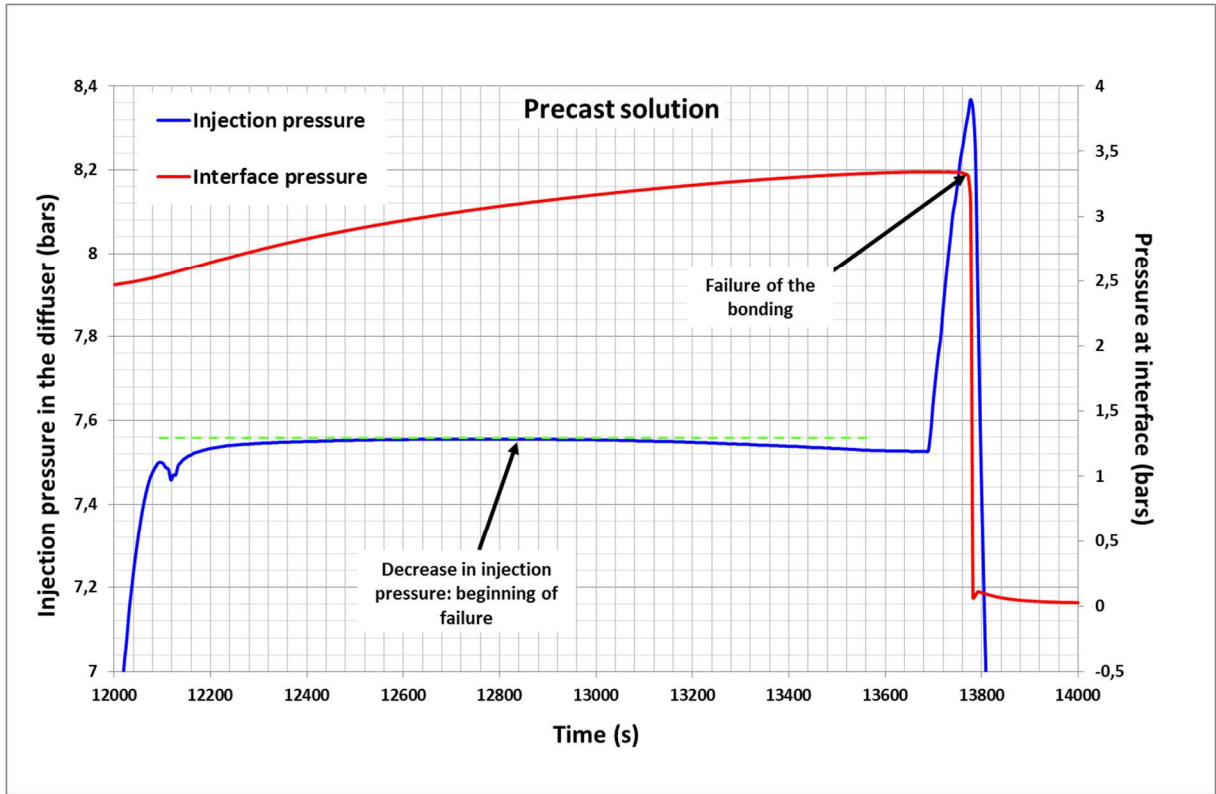
185 The experimental results obtained during the injection experiments are briefly described in the  
186 following. As expected, a decrease in gas flow rate (i.e. that required to achieve a given  
187 pressure in the diffusers) was measured, despite small gas leaks around the coating (see  
188 **Figure 7**). Gas leaks at the rear of the concrete slabs were difficult to evaluate. These results  
189 are directly related to the low gas permeability of the UHPFC – less than  $10^{-19} \text{ m}^2$ , and are not  
190 surprising. The flow rate into the diffusers was then progressively increased, in order to  
191 obtain a maximum gas pressure of 8 bars at the coating/wall interface. This value is specified  
192 by EDF, in order to provide for an acceptable safety margin with respect to the nominal  
193 relative pressure of 6.3 bars, which must be sustained by the coating/concrete interface of  
194 confinement structures, under accidental conditions.



195

196 *Figure 7: Gas flow bypassing the coating – detected by the application of soapy water.*

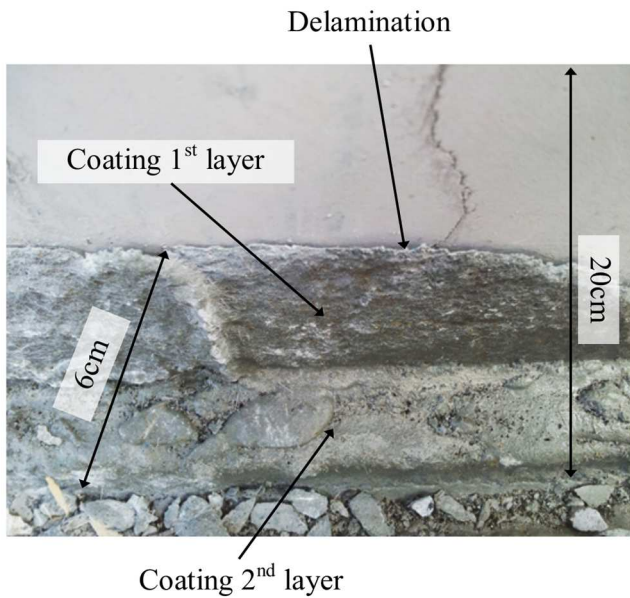
197 It was not possible to reach the specified pressure of 8 bars at the interface of both prototypes:  
198 the “in-situ cast” variant failed at 4.3 bars, and the pre-cast variant failed at 3.3 bars. These  
199 results confirm that the weak point of such a reinforcement technique is the bond quality of  
200 the interface. Any small initial defects (poor bonding over a small portion of the interface) can  
201 increase in size, as in the case of progressive opening of a crack, leading to a large  
202 delaminated surface, or even total delamination of the interface. Extensive delamination was  
203 detected for both cases using wave propagation techniques. The gas pressure measurements –  
204 made at the end of the injection tests - are shown in **Figure 8** for the pre-cast solution. The  
205 injection pressure started to decrease after reaching 7.55 bars at  $t \approx 12700$  s. A sharp increase  
206 in injection pressure, achieved by means of a rapid increase in injection flow rate (peaking at  
207  $t = 13780$  s, in **Figure 8**) was thus applied, resulting in a negligible increase in interface  
208 pressure, which reached a maximum value of 3.3 bars, prior to its complete failure. The  
209 resulting delamination of the interface can be seen in **Figure 9**.



210

211 *Figure 8: Gas pressure measurements. A sudden drop in interface pressure (red line) occurred at 3.3 bars.*

212



213

214 *Figure 9: Coating delamination observed on the "in-situ cast" prototype.*

215       **3 Part 2- AN ALTERNATIVE METHOD INVOLVING THE SPRAYING OF**  
216       **WATER**

217       **3.1 Gas relative permeability and water spraying**

218 In practice, the design and construction of a coating made from concrete or a polymer, for an  
219 in-situ application, can be a highly complex, costly and difficult exercise. Earlier tests made  
220 by our laboratory have shown that it is very difficult to design such a zero defect solution for  
221 a confining structure (i.e. for a very large surface area).

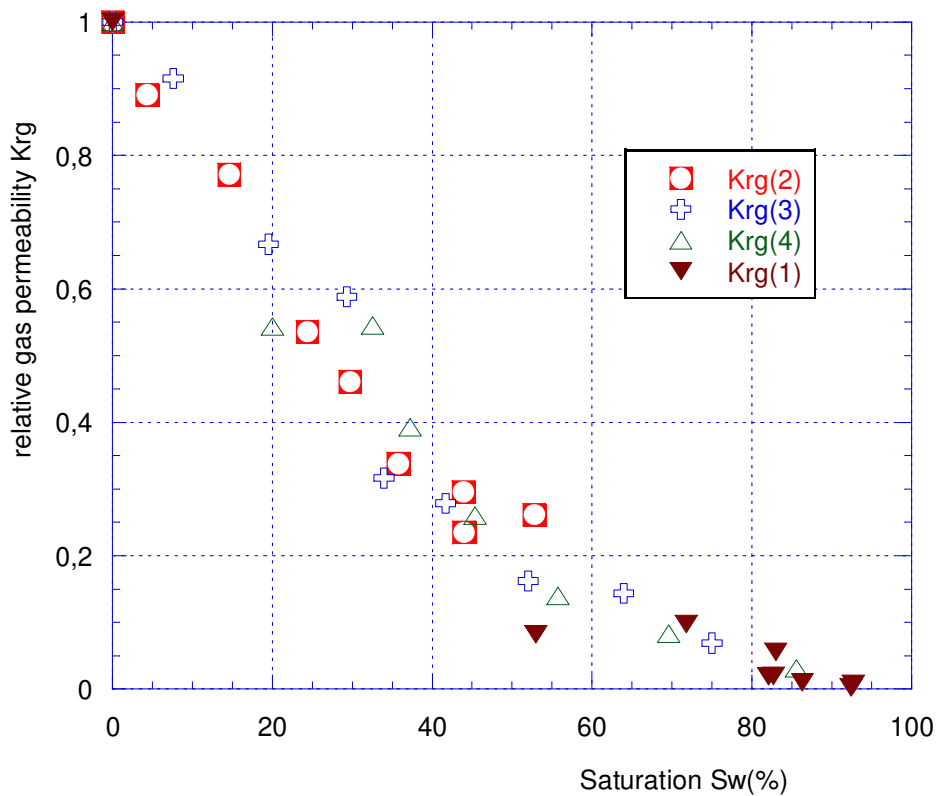
222 A different approach was thus suggested: why not simply spray water onto the confining  
223 structure in order to re-saturate the concrete, thereby globally decreasing its gas structure  
224 permeability? This simple technique would have a minimal cost when compared to many  
225 coating techniques, and can be implemented with no particular difficulties. Numerous  
226 experiments have been carried out to measure the relative (or effective) gas permeability of  
227 concrete in our laboratory [4,9], and elsewhere. These have shown that a sharp decrease in gas  
228 permeability occurs when the water saturation is increased. This phenomenon is consistently  
229 observed in cohesive porous media, and experiments carried out in our laboratory have shown  
230 that a significant decrease in gas permeability occurs even when the material is cracked [13].

231 A typical gas relative permeability curve is shown in **Figure 10**, for the case of intact  
232 concrete.

233 These results indicate that, depending on the characteristics of its porous structure, the gas  
234 relative permeability ( $K_{rg}$ ) of concrete can decrease by two (or three) orders of magnitude,  
235 when the matrix changes from the dry state to 80% water saturation ( $S_w$ ).

236 On the other hand, in the case of the water spraying technique, various issues such as possible  
237 chemical degradation, i.e. mostly alkali-aggregate reactions or sulphate attacks, must be taken

238 into account. EDF is currently running several dedicated studies to evaluate the level of risk,  
239 as well as the impact of spraying alkaline water onto a concrete structure. However, as the  
240 thickness of a real confining structure is 1.20 m, the water's depth of penetration would be  
241 limited to not more than 20-25 cm, i.e. to zones that were hardly affected by the increase in  
242 temperature caused by the initial concrete hydration. If used, the spraying device would be  
243 implemented between the two envelopes (see fig.1). The temperature into this zone is  
244 generally comprised between 25-30°C with a relative humidity level of around 50% (data  
245 provided by EDF).



246

247 *Figure 10: Relative gas permeability for four different concretes [3].*

248

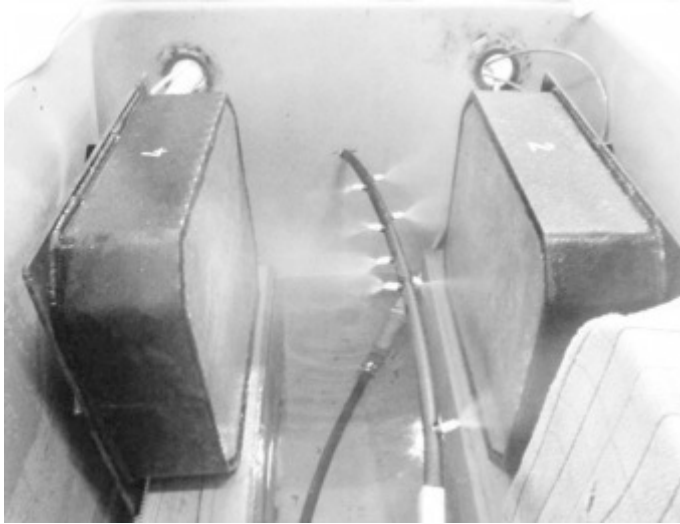
249       **3.1 Preliminary study: experimental campaign on concrete cylinders and on**  
250               **slabs**

251  
252   In a preliminary study, and prior to performing tests on the wall, three main aspects of the  
253   water-spraying process were investigated: the kinetics of imbibition, the increase in water  
254   saturation (and its deepness) and the following decrease in gas permeability. Experiments,  
255   described below, were carried out on concrete cylinders or slabs. They were composed with  
256   the same concrete as the wall. The experiments conducted on cylinders mainly aimed at  
257   following the water saturation evolution along their axis and the induced decrease in effective  
258   gas permeability. Those, conducted on slabs, were more global and intended to highlight that,  
259   despite a concreting joint, there is a large decrease in permeability after water spraying.

260       **3.1.1 Sample preparation and spraying system**

261   More than 35 cylinders, 65 mm diameter and 50 cm long, were cored from 2 month old  
262   concrete cubes and then cured at 50% RH and at a temperature of 25°C during 6 months.  
263   Their water saturation at this stage was approximately 45%. The initial gas permeability, used  
264   as a reference value, was measured on different samples after curing. Their lateral surface had  
265   then received several coatings of a special paint to ensure their water tightness. Two slabs,  
266   50cm wide, 30cm high and 15cm thick, were also mould: in one piece for the first one and in  
267   two pieces for the second in order to obtain a concreting joint. The waiting time between the  
268   two concreting phases was 24h as a bad quality joint was targeted. They were cured in water  
269   at 25°C for 2 months then cured at 50% RH and at a temperature of 25°C during 6 months.  
270   Following this step they were glued onto a steel frame, allowing the measurement of their gas  
271   permeability.

272 Their water saturation was increased by spraying them with water for several weeks (**Figure**  
273 **11**). The same arrangement was also used to spray water onto concrete test cylinders (**Figure**  
274 **12**). As their lateral surface was initially sealed with glue, the saturation of these cylinders  
275 was thus achieved axially via their flat ends. Spraying was achieved by means of electric  
276 pumps and a small spray-pipe system.



277

278 *Figure 11: Two concrete slabs during spraying.*



279

280 *Figure 12: Water spraying of concrete cylinders stored above the collected water.*

281

### 282 3.1.2 Testing methodology

283

284 Slices of the cylinder were periodically cut in order to measure their water saturation and  
285 effective gas permeability. These operations allowed the water's depth of penetration, as well  
286 as its efficiency in terms of any measured decrease in gas permeability, to be evaluated. The  
287 first of these slices were cut to a thickness of 15 mm, which was found to be insufficient,  
288 since large air bubbles, potentially affecting the permeability measurements, were sometimes  
289 trapped in the concrete (cf. Figure 13). A thickness of 30 mm was thus used for the remaining  
290 slices.



291

292 *Figure 13: bubbles in concrete slices.*

293 Imbibition was carried out in cycles: 15 min of spraying, followed by 15 min without  
294 spraying. The first cylinder was cut into slices after 2 days of spraying, the next was tested  
295 after 7 days, and the remaining cylinders were tested every 15 days. Each cylinder was  
296 weighed and sawn, and the following measurements were made on every slice:

- 297 • (1) Weighing
- 298 • (2) Effective gas permeability measurement
- 299 • (3) Drying at 65°C followed by weighing

- 300 • (4) Intrinsic (or dry) gas permeability measurement
- 301 • (5) Water saturation under vacuum, in order to determine the water saturation  $S_w$  at
- 302 step (1)

303 From these measurements, the water saturation and gas permeability of the cylinders could be  
304 determined as a function of distance from the surface exposed to spraying. As mentioned  
305 before, gas permeability measurements are usual operations conducted in our laboratory and  
306 can be found in [3]. The dry permeability was measured after a drying at 65°C. This  
307 temperature is a choice (or a compromise) made to avoid additional micro-cracking that can  
308 occur at higher drying temperature i.e. 105°C.

309 The slabs were simply sprayed for 70 days (15mn of spraying – 15mn without spraying) and  
310 their gain in mass and decrease in permeability periodically measured.

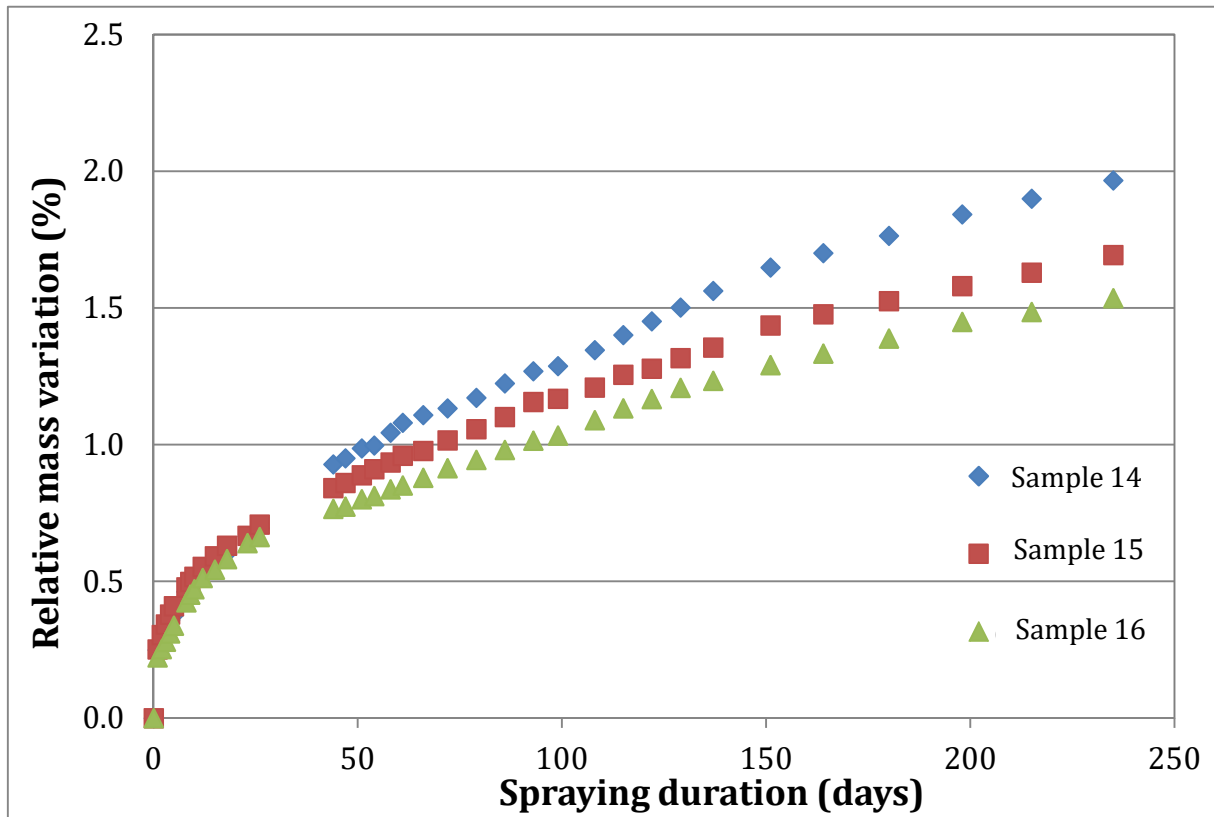
## 311 3.2 Results

### 312 3.2.1 Gain in mass for the cylindrical samples

313 The relative increase in mass of three control samples was measured for 240 days. **Figure 14**  
314 plots the results as a function of spraying time. Initially, their mass increased very quickly due  
315 to the effects of capillary water absorption, following which the rate of mass change  
316 decreased progressively over time. It is assumed that this phenomenon is initially controlled  
317 by capillarity, since it is quite rapid. As the concrete water saturation, close to the sprayed  
318 end, increases, the water penetration through this zone will be more and more controlled by  
319 the water concrete permeability. It is then supposed that this could significantly reduce the  
320 water flow rate i.e. the gain in mass [14].

321 The global increase in mass of the three samples ranged between 1.5% and 2%. The  
322 dispersion in these values can probably be explained by small differences in porosity, or the

323 presence of bubbles. Fifty percent of the mass increase was obtained after the first 50 days. It  
324 confirms that imbibition, with liquid water, occurs significantly faster than drying that is  
325 mainly a diffusive phenomenon.



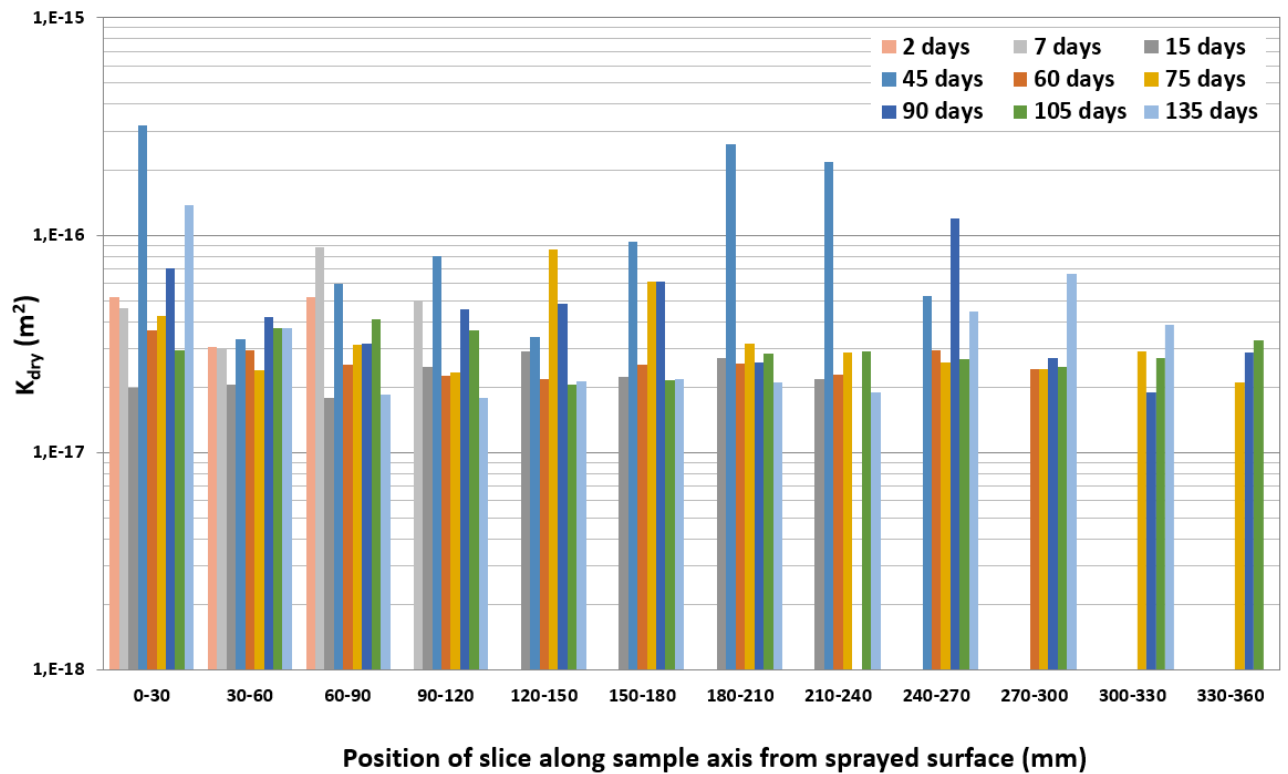
326

327 *Figure 14: Relative mass variation for three control samples.*

### 328 3.2.2 Gas permeability of the cylindrical samples

329 Gas permeability measurements were made using sample slices cut from ten different  
330 cylinders. These cylinders had been sprayed with water for different periods of time (up to  
331 135 days). Their effective gas permeability was measured first. This corresponds to that of  
332 partially saturated concrete. The slices were then dried at 65°C, until their mass reached a  
333 stable value, allowing their dry (or intrinsic) gas permeability to be measured. The resulting  
334 values are plotted in **Figure 15**, for slices identified as a function of their original location  
335 (axial depth) inside their parent cylinder. It is important to note that the dry permeability of

336 these samples is nearly homogeneous as a function of depth. The mean gas permeability is  
 337 found to be approximately  $2.5 \cdot 10^{-17} \text{ m}^2$ , however some of the cylinders had contrasted  
 338 properties, when compared with this average value. This is the case for the cylinder sawn  
 339 after 45 days of spraying, since its permeability was ten times greater than the average value.  
 340 This kind of dispersion is frequently met for in-situ structures.



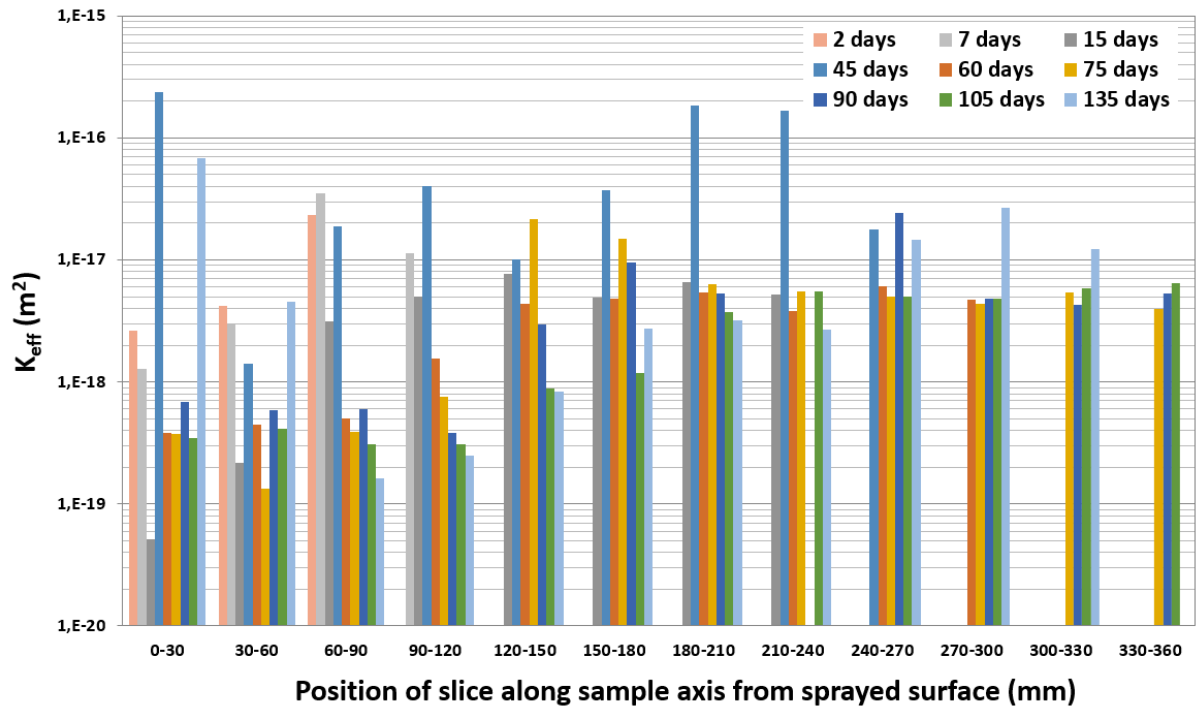
341 **Position of slice along sample axis from sprayed surface (mm)**

342 *Figure 15: Dry gas permeability of concrete slices (30 mm thick) taken from 9 different cylindrical samples (each with a*  
 343 *different spraying duration). The position of each slice along its parent cylinder is measured from the sprayed end surface of*  
 344 *the cylinder.*

345 Before being dried, the effective gas permeability of the partially saturated slices was  
 346 measured. The full set of results is shown in **Figure 16**. Some samples are atypical, since their  
 347 gas permeability remains very high, despite a high level of saturation (close to 90%, see  
 348 further). Although the origin of this phenomenon has not yet been identified, we assume that  
 349 these samples contained very large pores and cracks along their length, which even at high

350 levels of saturation were not completely filled with water. These disparities are more visible  
351 in **Figure 17**, showing the relative gas permeability of all slices. The relative permeability  
352  $K_{rg}$  is calculated as the ratio  $K_{eff}/K_{dry}$ , where the effective and dry permeability are  
353 measured on the same sample. Overall, there is a strong decrease in relative permeability at  
354 depths as great as 18 cm below the outer surface of the cylinders, providing evidence that  
355 spraying could be used to decrease the permeability of the entire wall. In Figure 18 the  
356 relative gas permeability of the different slices is shown as a function of water saturation. A  
357 complementary study was carried out to complete this figure with a “real” relative  
358 permeability curve (red line). The term “real” means that saturation was obtained on samples,  
359 prepared under various conditions of relative humidity, until their mass stabilised at a constant  
360 value. Under these conditions, water saturation is considered to be uniform throughout the  
361 samples. Although it was expected that spraying would lead to layered saturation effects, and  
362 despite some atypical results, there is a very close match between the “homogeneous relative  
363 permeability” curve (red line) and the relative permeability obtained after spraying (remaining  
364 points in this figure). This means that homogeneous saturation was achieved across the  
365 samples' full thickness, after a relatively small number of days.

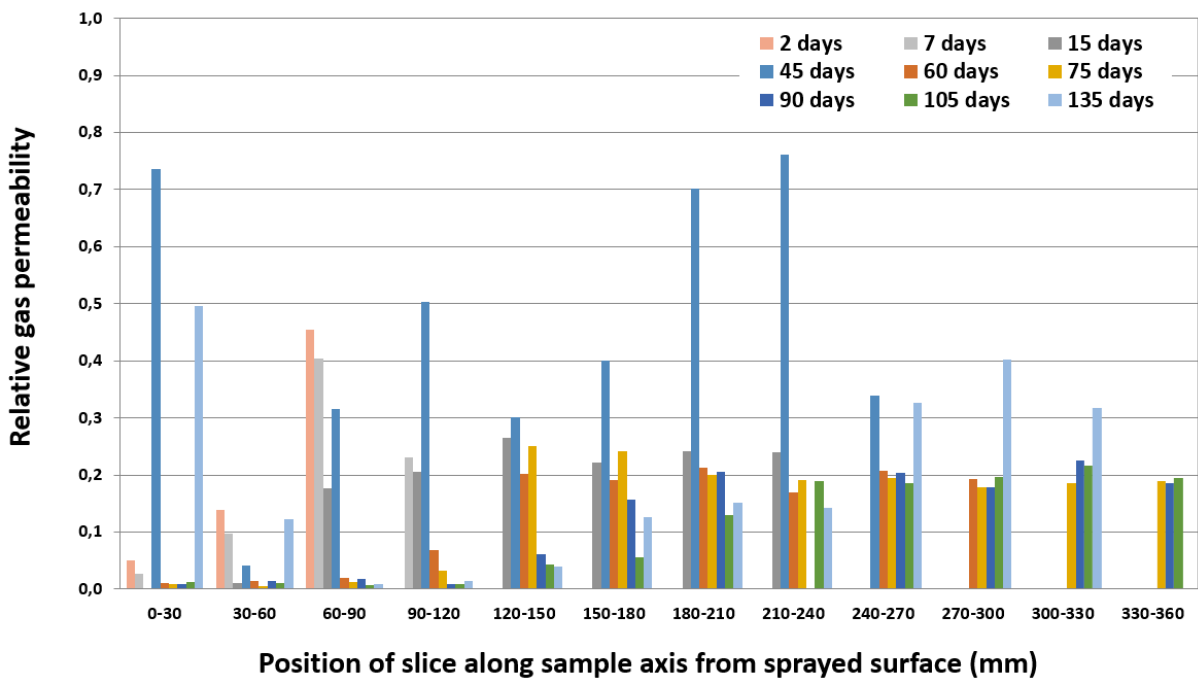
366



367

368 *Figure 16: Effective gas permeability of 30 mm slices of concrete as a function of their distance (measured from the sprayed*

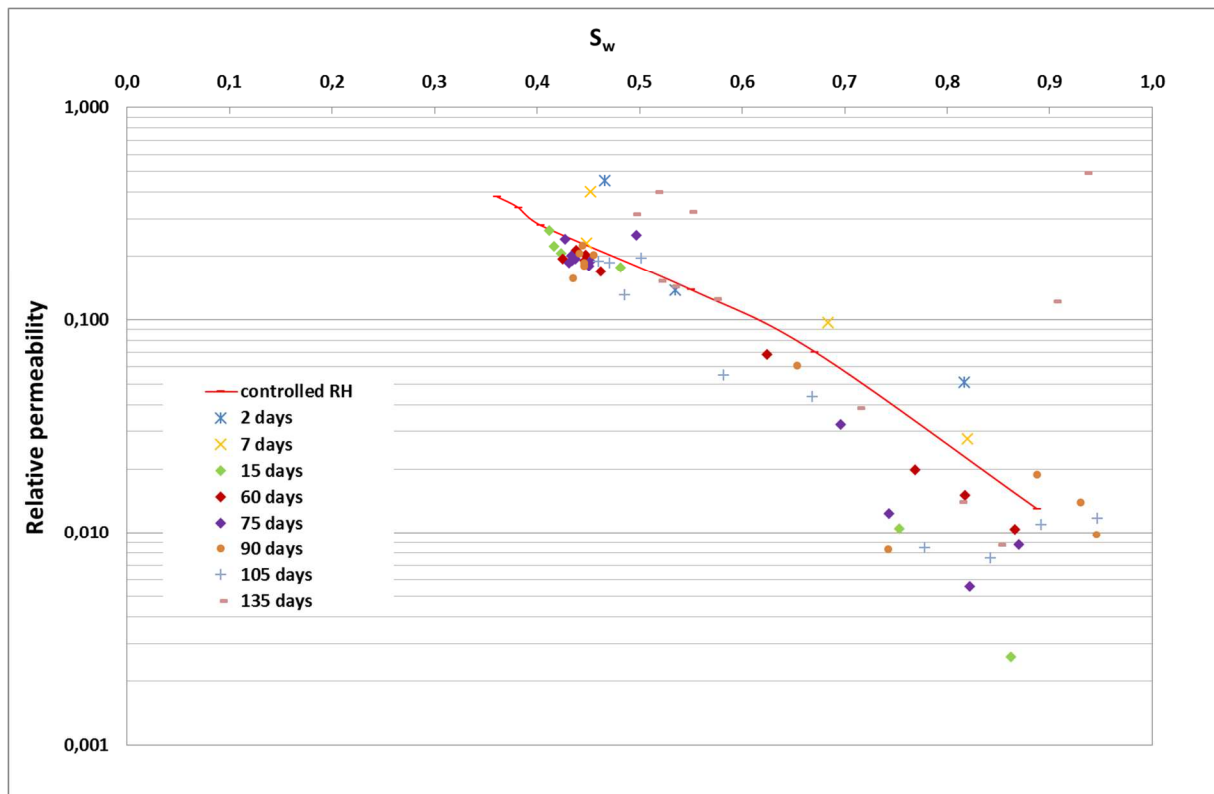
369 *surface of the original sample), and the spraying duration*



370

371 *Figure 17: Relative gas permeability of 30 mm slices of concrete as a function of their distance (measured from the sprayed*

372 *surface of the original sample), and the spraying duration*



373

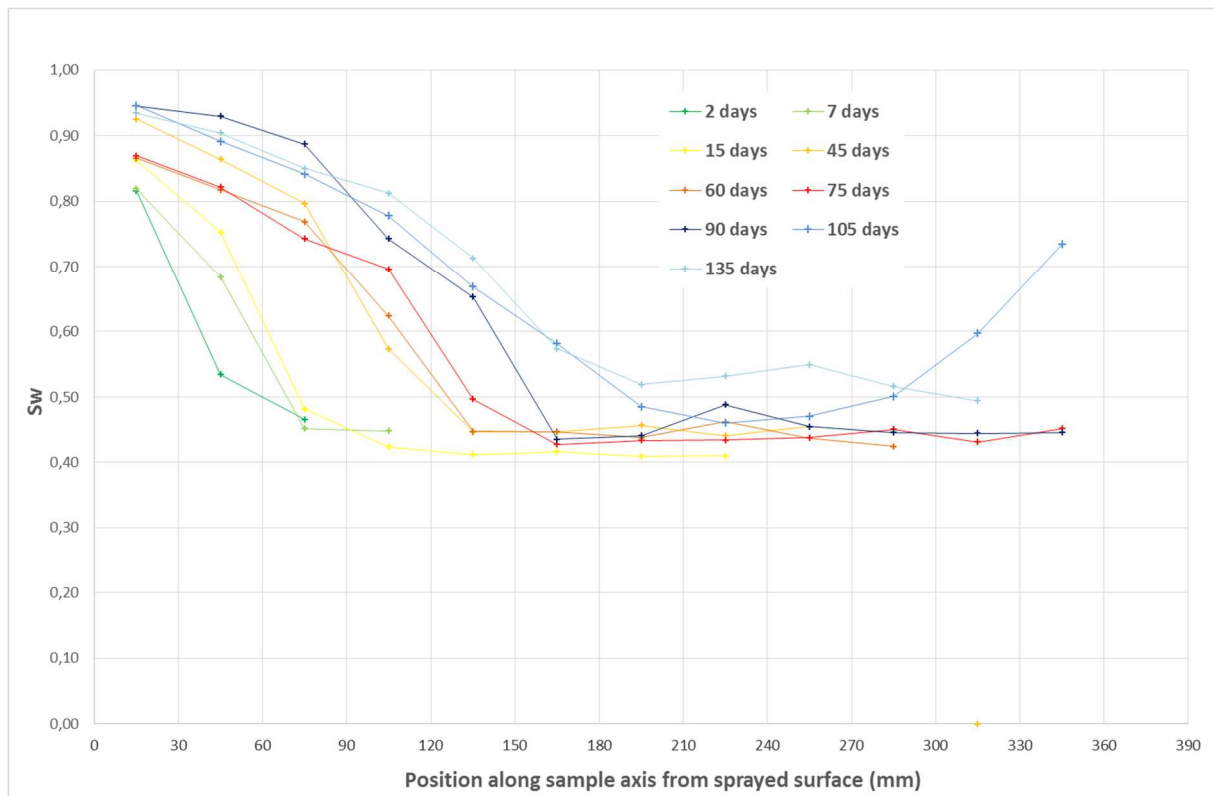
374 *Figure 18: Semi-log representation of the relationship between relative permeability and water saturation ( $S_w$ ), measured on*  
 375 *slices of sprayed samples, and on samples stored under controlled relative humidity conditions (RH controlled using a brine*  
 376 *solution).*

### 377 3.2.3 Water saturation of the cylindrical samples

378 The water front propagation kinetic is presented in Figure 19, which plots the material's water  
 379 saturation as a function of distance from the sprayed surface and spraying time. The initial  
 380 values of saturation lie in the range between 40-50%, with a mean value of 45%. Some  
 381 scattering can be observed in this data, resulting from the typical dispersion of porous  
 382 structures in cementitious materials. Imbibition and saturation increase rather quickly, since in  
 383 the zone situated 30-40 mm below the sprayed surface, the saturation reaches more than 70%  
 384 after 15 days of spraying. After 90-105 days of spraying, this relatively highly saturated zone  
 385 extends to a distance of 120-130 mm from the sprayed surface, and the 30-40 mm zone  
 386 reaches more than 90% saturation. After 135 days, the partially saturation zone has extended

387 to more than 240 mm from the sprayed surface, and a concrete thickness of at least 120 mm is  
 388 highly saturated. The latter value represents approximately 10% of a confining structure's  
 389 thickness, and could be sufficient to considerably reduce the gas permeability of the entire  
 390 structure. A simple calculation shows that if the relative gas permeability of the 120 mm zone  
 391 is approximately 1% (assuming water saturation of the concrete greater than 80% - see Figure  
 392 19), the gas permeability of the overall structure would be 2 to 3 times lower than before  
 393 spraying. This technique could thus be a viable solution for the recovery of a significant  
 394 proportion of the gas tightness of reactor confining structures.

395



396

397 *Figure 19: Water saturation distribution as a function of distance from the sprayed surface, and spraying duration.*

398

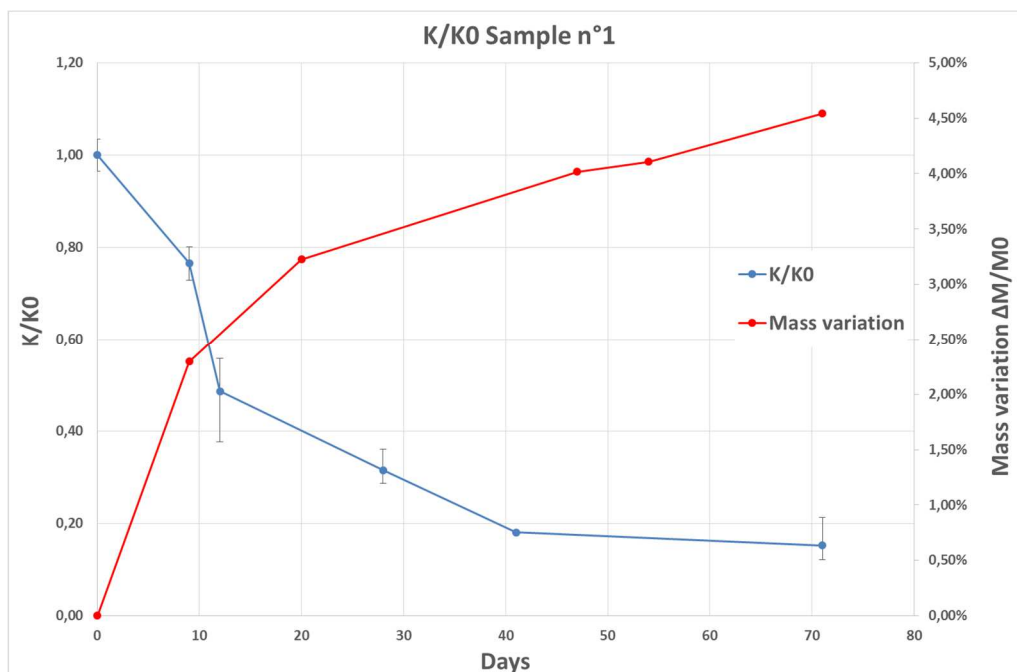
399 **3.2.1 Results obtained on slabs**

400

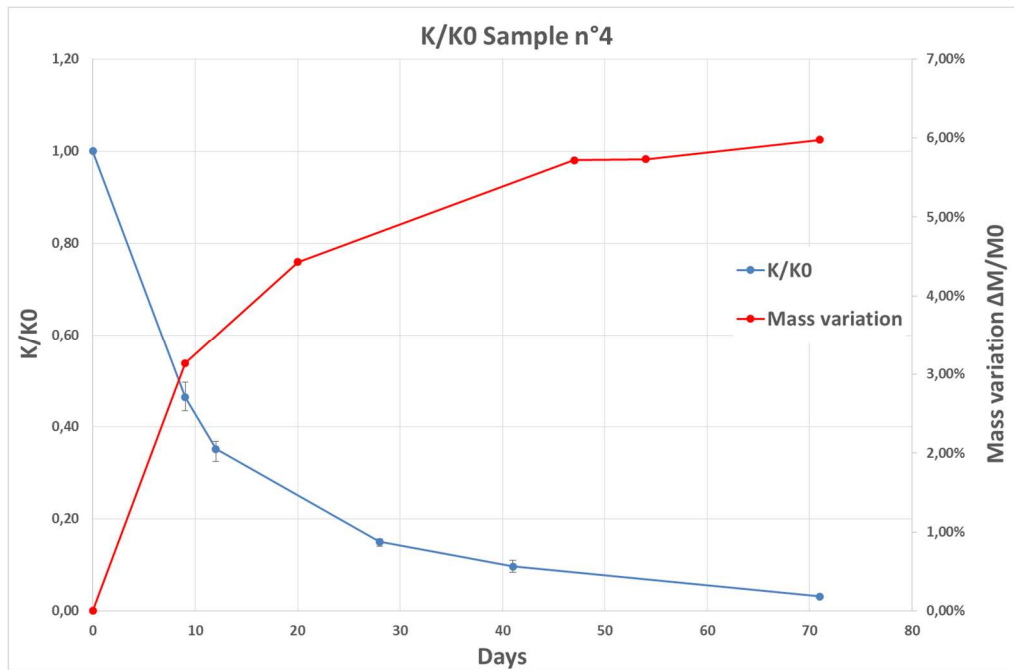
401 As the spraying process may be insufficient to counter the effects produced by cracked zones,  
402 or zones with concreting joints that can lead to high leakage rates, additional tests were made  
403 with concrete plates presented before.

404 The initial gas permeability  $K_0$  (i.e. before spraying) was first measured on each slab. For the  
405 slab with no concreting joint,  $K_0$  was found to be  $7.8 \cdot 10^{-18} \text{ m}^2$ . The gas permeability of the  
406 slab with a concreting joint was two orders of magnitude higher ( $K_0 = 1,5 \cdot 10^{-15} \text{ m}^2$ ). This  
407 strong difference comes from the “bad” joint quality, which behaves almost like a macro-  
408 crack. The influence of spraying on the mass and gas permeability of the slab with no  
409 concreting joint is plotted in Figure 20 : its permeability is found to decrease by a factor of 5  
410 after only 6 weeks of imbibition. A much stronger decrease, by a factor of 20, is also observed  
411 for the slab with concrete joints (see Figure 21). This is evidence that the water spraying  
412 operation is efficient even in the case of a damaged material.

413



414 *Figure 20: Decrease in permeability (K/Ko) and mass variation (M/Mo) vs. spraying duration for sample 1.*



415

416 *Figure 21: Decrease in permeability (K/Ko) and mass variation (M/Mo) vs. spraying duration for sample 2 (with a concrete*  
417 *joint).*

### 418 **3.3 Improvement in gas tightness obtained by spraying the experimental wall** 419 **with water**

420 The encouraging results described above led to the design of a dedicated system allowing  
421 water to be sprayed onto the third portion of the wall, which had not been used for the testing  
422 of coating solutions. Figure 22 is a map of the third portion of the wall, showing the positions  
423 of gas diffusers (black dotted lines and green numbers) and the main leakage areas  
424 (continuous red lines, identified with a bubbling agent).

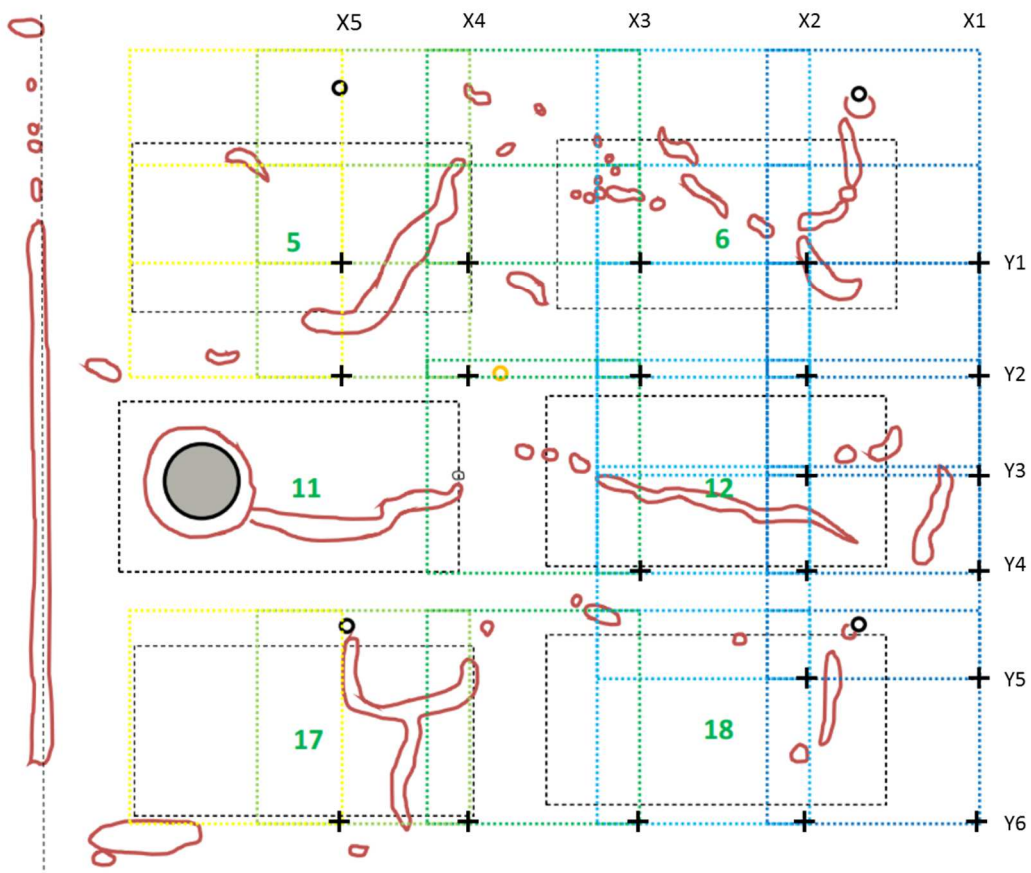
425 The wall's initial gas permeability was mapped approximately 1.5 years after it was cast,  
426 using a tight, square cover (approximately 0.55 x 0.55 m) equipped with a mass flow meter.  
427 The gas pressure in the diffusers was increased to approximately 0.2 MPa (absolute pressure),  
428 and once steady state conditions had been reached, variations in flow rate were used to

429 evaluate the gas permeability of different portions of the wall. Table 2 provides the measured  
430 values of apparent gas permeability ( $\times 10^{-18} \text{ m}^2$ ) of these different zones, together with their  
431 coordinates ( $X_i, Y_i$ ) shown in Figure 22, with the corresponding black crosses indicating the  
432 position of the right bottom corner of the cover during the test.

433 The results in **Table 2** reveal a strong dispersion in gas permeability, which ranges from  
434  $0.7 \cdot 10^{-18} \text{ m}^2$  to  $446.10^{-18} \text{ m}^2$ . This is due to drying shrinkage of the wall, which was built using  
435 “poor” quality concrete. This particular type of concrete, made with a high water-to-binder  
436 ratio, was selected for practical and scheduling reasons, in order to improve the drying  
437 kinetics of the concrete and to obtain high (more easily measurable) values of permeability.  
438 As a consequence, large drying cracks formed, especially on the sides of the wall, due to  
439 structural effects. Examples of these cracks are shown in the optical microscope enlargements  
440 of Figure 23, Figure 24, Figure 25, Figure 26 **and** Figure 27. Some of the cracks, such as that  
441 shown in Figure 23, reached a width of  $800\mu\text{m}$ , thus explaining the high gas permeability of  
442 areas X1Y4 and X1Y5. The widths of the other cracks shown in these images are:  
443 approximately  $500\mu\text{m}$  in **Figure 24** (area X1Y6),  $140\mu\text{m}$  in Figure 25 (areas X1Y1 and  
444 X1Y2),  $200\mu\text{m}$  in Figure 26 (area X4Y6), and from  $120$  to  $330\mu\text{m}$  in Figure 27 Figure 27  
445 (areas X2Y5 and X2Y4). No clear correlation was found between the appearance of the  
446 cracks and their corresponding gas permeability, mainly because they were observed only  
447 superficially, and their depth and length were not determined.

448 The gas permeability of this slab was measured again after 49 days of intermittent water  
449 spraying (5 min per hour). The spraying device was similar to that used previously on  
450 concrete slabs (Figure 11). Table 3 shows the measured values of apparent gas permeability  
451 and their variations when compared to the initial results. These results should be treated with  
452 caution, as there are some significant sources of uncertainty. Nevertheless, an average

453 decrease of 52% in gas permeability is obtained, with a significant degree of dispersion. It can  
454 be seen that the initial level of permeability is partially correlated with the decrease in  
455 permeability after spraying. This outcome was expected, since it is much more difficult to  
456 create gas tightness in a macro-cracked area because large cracks are subjected to very fast  
457 drying, and the injected gas pressure, generated during the test, can be greater than the local  
458 capillary forces, and thus sufficient to drive any remaining water out of the crack.



459  
460 *Figure 22: map of the test wall showing the main flow paths (continuous red lines), position of the gas diffusers (black*  
461 *rectangles drawn in dotted lines), and zones where the permeability is measured (blue, green and yellow rectangles drawn in*  
462 *dotted lines), identified by their corresponding X and Y coordinates.*

463

464

465

466

467

468

469

<b>X5Y1</b>	<b>X4Y1</b>	<b>X3Y1</b>	<b>X2Y1</b>	<b>X1Y1</b>
<b>1.0</b>	9.1	3.6	2.8	52.0
<b>X5Y2</b>	<b>X4Y2</b>	<b>X3Y2</b>	<b>X2Y2</b>	<b>X1Y2</b>
<b>1.2</b>	8.5	9.5	3.2	30.3
			<b>X2Y3</b>	<b>X1Y3</b>
			0.7	2.4
		<b>X3Y4</b>	<b>X2Y4</b>	<b>X1Y4</b>
		5.1	7.8	255.6
			<b>X2Y5</b>	<b>X1Y5</b>
			1.9	446.5
<b>X5Y6</b>	<b>X4Y6</b>	<b>X3Y6</b>	<b>X2Y6</b>	<b>X1Y6</b>
<b>0.9</b>	181.0	14.4	27.2	371.6

470 *Table 2: initial apparent gas permeability (x 10<sup>-18</sup> m<sup>2</sup>) of selected zones on the wall, identified by their XiYj coordinates.*

471

472

473

474

475

476

<b>X5Y1</b>	<b>X4Y1</b>	<b>X3Y1</b>	<b>X2Y1</b>	<b>X1Y1</b>
<b>0.1 (-87%)</b>	3.2 (-65%)	4.3 (+17%)	1.7 (-38%)	11.3 (-78%)
<b>X5Y2</b>	<b>X4Y2</b>	<b>X3Y2</b>	<b>X2Y2</b>	<b>X1Y2</b>
<b>0.1 (-92%)</b>	5.6 (-34%)	4.0 (-58%)	1.7 (-45%)	7.9 (-74%)
			<b>X2Y3</b>	<b>X1Y3</b>
			0.2 (-74%)	0.9 (-64%)
		<b>X3Y4</b>	<b>X2Y4</b>	<b>X1Y4</b>
		2.5 (-52%)	5.0 (-37%)	122.8 (-52%)
			<b>X2Y5</b>	<b>X1Y5</b>
			1.2 (-38%)	424.6 (-5%)
<b>X5Y6</b>	<b>X4Y6</b>	<b>X3Y6</b>	<b>X2Y6</b>	<b>X1Y6</b>
<b>1.7 (+74%)</b>	16.9 (-91%)	5.7 (-60%)	2.3 (-91%)	6.2 (-98%)

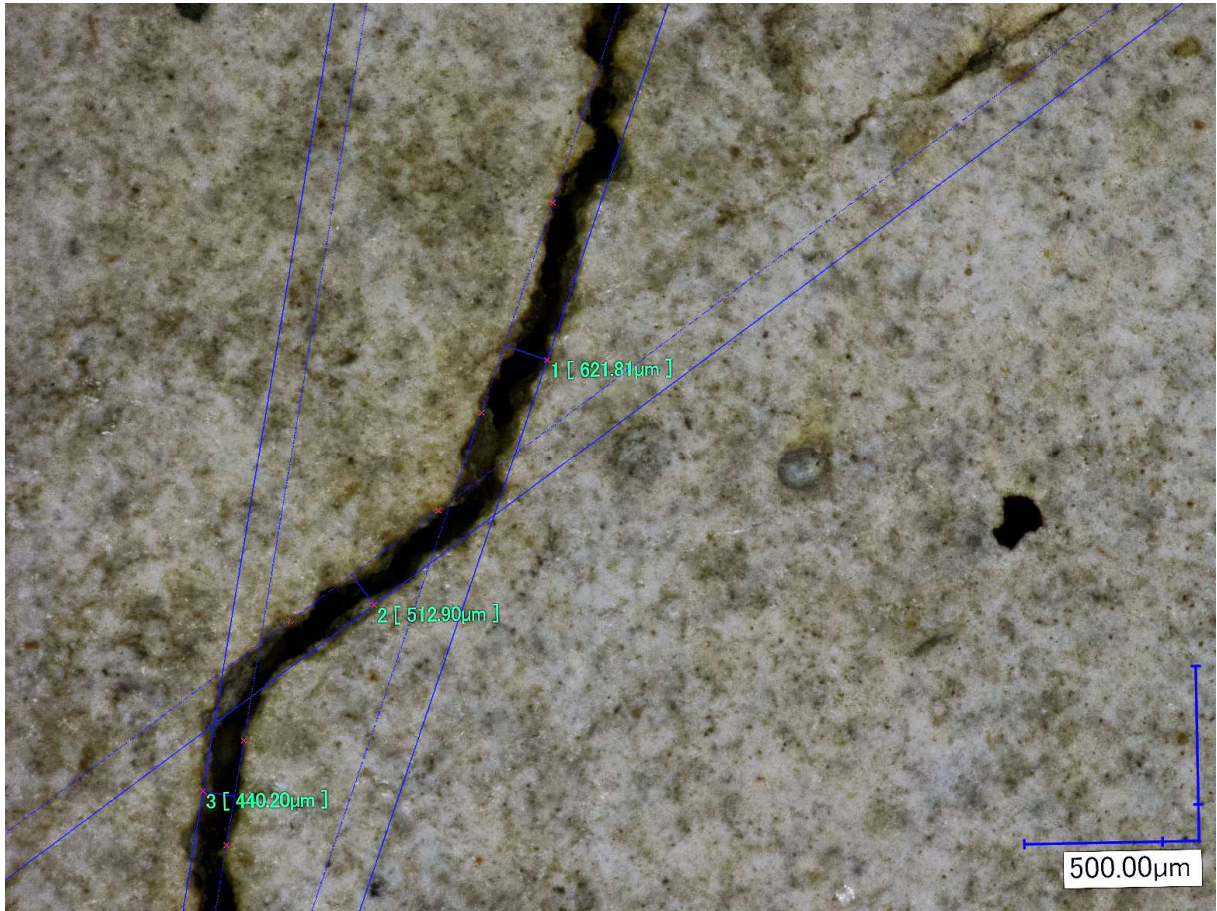
477 *Table 3: apparent gas permeability ( $\times 10^{-18} \text{ m}^2$ ) of different zones (identified by their  $X_iY_j$  coordinates) on the wall following*478 *49 days of water spraying, and corresponding variations (%) with respect to the initial permeability.*

479



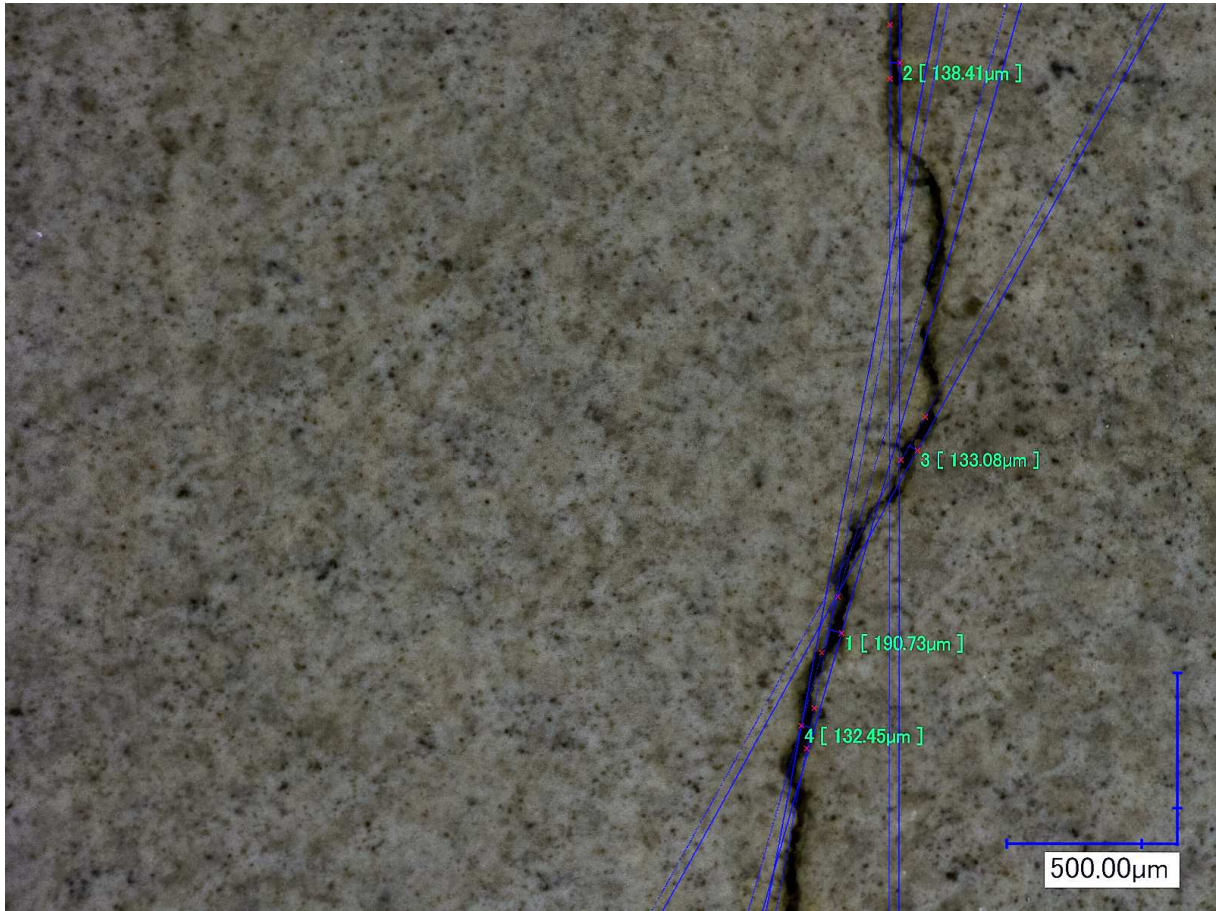
480

481 *Figure 23: drying crack in the XIY4 and XIY5 measurement zones.*



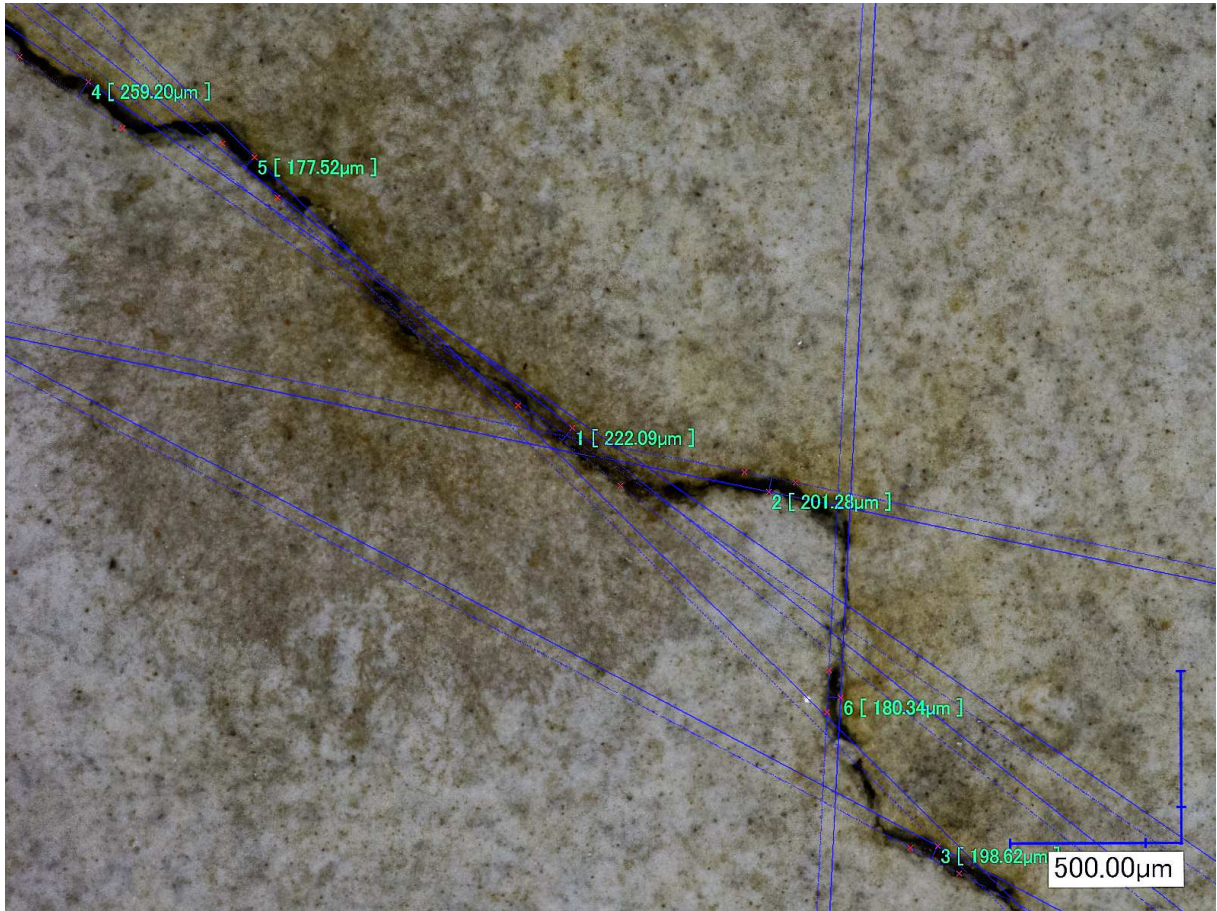
482

483 *Figure 24: drying crack in the XIY6 measurement zone.*



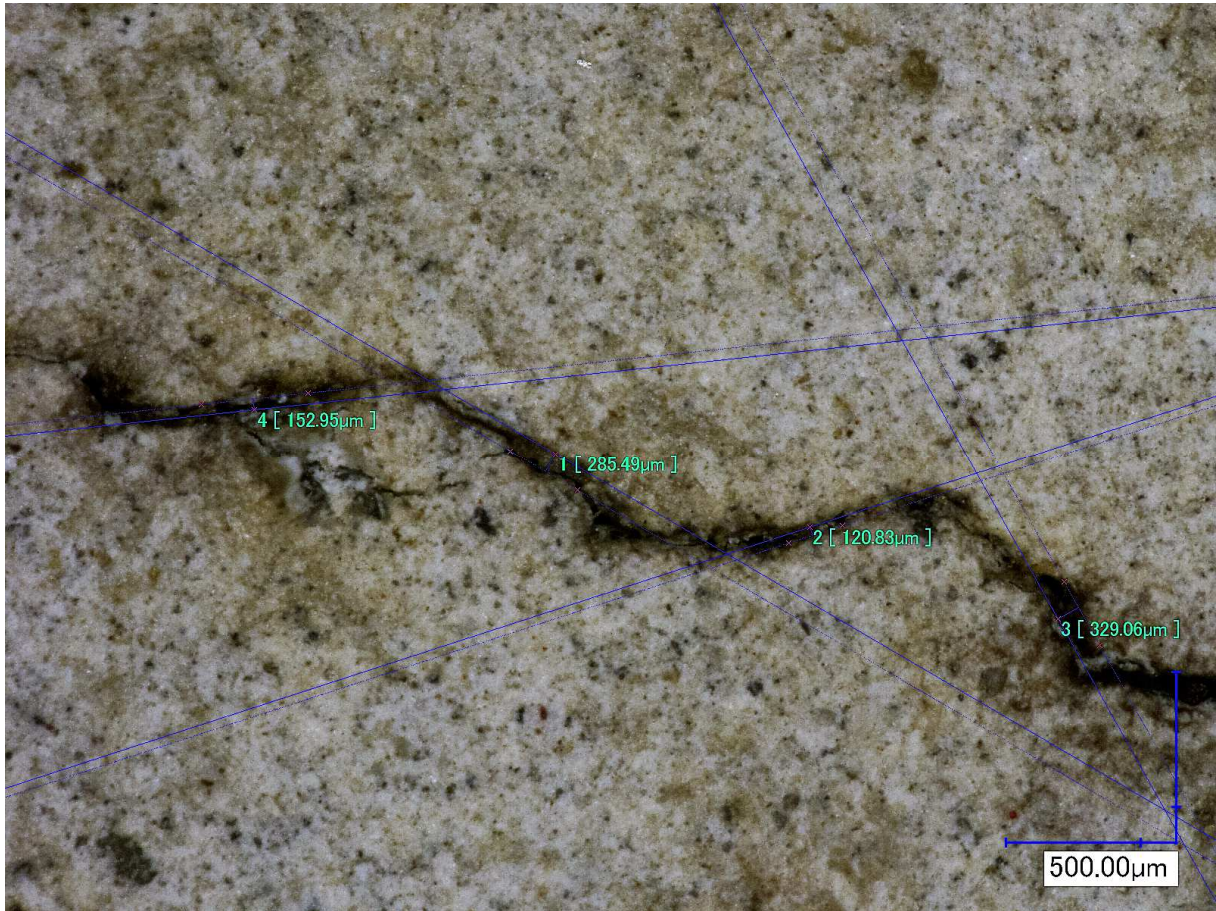
484

485 *Figure 25: drying crack in the XIY1 and XIY2 measurement zones.*



486

487 *Figure 26: drying crack in the X4Y6 measurement zone.*



488

489 *Figure 27: drying crack in the X2Y5 and X2Y4 measurement zones.*

490

#### 491 **4 Conclusions**

492 In the present study the design of a test wall is presented and discussed: this unique specimen  
493 was designed to reproduce gas transfer and pressure conditions similar to those encountered  
494 in the confinement structures of current French nuclear power plants. The test wall has three  
495 distinct zones, which can be modified through the use of reinforcement coating solutions,  
496 designed to improve the gas tightness of the external surface of such confinement structures.  
497 Two potential UHPFC coating solutions were tested, and were found to fail before reaching  
498 the target gas pressure of 4 bars (increased by a safety margin). This provides evidence that,

499 whatever the chosen coating technology, the most crucial issue will be the bonding strength at  
500 the interface between the wall and the coating. A different approach to the improvement of  
501 confinement structure gas tightness has therefore been studied that is based on the use of  
502 water spraying to decrease the relative gas permeability of micro-cracked concrete. Initial  
503 water spraying experiments on cylinders and concrete slabs have produced very promising  
504 results:

- 505 1- imbibition by spraying penetrates very quickly into the concrete
- 506 2- this leads to a strong decrease in gas permeability
- 507 3- even if the slab has a “bad quality” concreting joint, its gas permeability is  
508 considerably reduced (by a factor 20) after water spraying.

509 An experiment made with a concrete wall mock-up shows that the structure's gas permeability  
510 was reduced, on average, by 52% even in macro-cracked areas.

511 A more universal strategy could combine water spraying, which significantly reduces the  
512 concrete's gas permeability, with local repairs based on the application of polymers to the  
513 structure's outer surface. It remains to be verified that re-saturation does not lead to  
514 detrimental chemical reactions within the concrete structure.

515

516 Acknowledgments

517 The authors wish to thanks Electricity Of France (EDF) for scientific and financial support.

518

519 References

- 520 [1] A. Abbas, M. Carcasses and J.-P. Ollivier , Gas permeability of concrete in relation to its  
521 degree of saturation, *Materials and Structures/Matériaux et Constructions*, Vol. 32, January-  
522 February 1999, pp 3-8. 1359-5997/99 © RILEM SCIENTIFIC REPORTS.
- 523 [2] V. Baroghel-Bouny, Water vapour sorption experiments on hardened cementitious  
524 materials. Part II: Essential tool for assessment of transport properties and for durability  
525 prediction, *Cement and Concrete Research*, Volume 37, Issue 3, March 2007, Pages 438-454.
- 526 [3] W. Chen, J. Liu, F. Brue, F. Skoczylas, C.A. Davy, X. Bourbon, J. Talandier, Water  
527 retention and gas relative permeability of two industrial concretes, *Cement and Concrete*  
528 *Research*, Volume 42, Issue 7, July 2012, Pages 1001-1013.
- 529 [4] X.T. Chen, G. Caratini, C.A. Davy, D. Troadec, F. Skoczylas, Coupled transport and poro-  
530 mechanical properties of a heat-treated mortar under confinement, *Cement and Concrete*  
531 *Research* 49:10–20 · July 2013.
- 532 [5] W. Wang, J. Liu, F. Agostini, C.A. Davy, F. Skoczylas, D. Corvez, Durability of an Ultra  
533 High Performance Fiber Reinforced Concrete (UHPFRC) under progressive aging, *Cement*  
534 *and Concrete Research* 55(1):1–13 · January 2014.
- 535 [6] Z.A. Kameche, F. Ghomari, M. Choinska, A. Khelidj, Assessment of liquid water and gas  
536 permeabilities of partially saturated ordinary concrete, *Construction and Building Materials*,  
537 Vol. 65, 29 August 2014, Pages 551-565
- 538 [7] F.D. Lydon, The relative permeability of concrete using nitrogen gas, *Construction and*  
539 *Building Materials*, Vol. 7, Issue 4, December 1993, Pages 213-220
- 540 [8] R. Cortas, E. Rozière, S. Staquet, A. Hamami, A. Loukili, M.-P. Delplancke-Ogletree,  
541 Effect of the water saturation of aggregates on the shrinkage induced cracking risk of concrete  
542 at early age, *Cement and Concrete Composites*, Vol. 50, July 2014, Pages 1-9

- 543 [9] J. Liu, F. Agostini, F. Skoczylas, From relative gas permeability to in situ saturation  
544 measurements, *Construction and Building Materials*, Vol. 40, March 2013, Pages 882-890
- 545 [10] S. Michel-Ponnelle, Validation of the models of drying on a cylindrical Summarized  
546 concrete test-tube, Code\_Aster, Validation-V7, HSNA102, 2011. [http://code-  
547 aster.org/doc/v12/en/man\\_v/v7/v7.20.102.pdf](http://code-aster.org/doc/v12/en/man_v/v7/v7.20.102.pdf)
- 548 [11] B. A. Tayeh, B.H. Abu Bakar, M.A. Megat Johari, Yen Lei Voo, Evaluation of Bond  
549 Strength between Normal Concrete Substrate and Ultra High Performance Fiber Concrete as a  
550 Repair Material, *Procedia Engineering*, Volume 54, 2013, Pages 554-563, ISSN 1877-7058,  
551 <https://doi.org/10.1016/j.proeng.2013.03.050>.
- 552 [12] B.A. Tayeh, B.H. Abu Bakar, M.A. Megat Johari, Y.L. Voo, Mechanical and  
553 permeability properties of the interface between normal concrete substrate and ultra high  
554 performance fiber concrete overlay, *Construction and Building Materials*, Volume 36, 2012,  
555 Pages 538-548, ISSN 0950-0618, <https://doi.org/10.1016/j.conbuildmat.2012.06.013>.
- 556 [13] S. M'Jahad, C. A. Davy, X. Bourbon, F. Skoczylas, Water Retention and Gas Migration  
557 of Two High-Performance Concretes after Damage, *Journal of Materials in Civil Engineering*,  
558 American Society of Civil Engineers, 2015, *Sustainable Materials and Structures*, 27 (2),  
559 pp.A4014008. <10.1061/(ASCE)MT.1943-5533.0001028 >
- 560 [14] J. Liu, Etude expérimentale de la perméabilité relative des matériaux cimentaires et  
561 simulation numérique du transfert d'eau dans le béton, PhD thesis, December 13<sup>th</sup>, 2011,  
562 Centrale Lille, France, in French.
- 563 [15] L Granger, C.Y Rieg, J.P Touret, F Fleury, G Nahas, R Danisch, L Brusa, A Millard, C  
564 Laborderie, F Ulm, P Contri, K Schimmelpfennig, F Barré, M Firnhaber, J Gauvain, N

565 Coulon L.M.C Dutton and A Tuson, Containment Evaluation under Severe Accidents  
566 (CESA): synthesis of the predictive calculations and analysis of the first experimental results  
567 obtained on the Civaux mock-up. Nuclear Engineering and Design, Volume 209, Issues 1–3,  
568 November 2001, Pages 155-163.

569 [16] A. Spasojevic, Structural implications of ultra-high performance fibre-reinforced  
570 concrete in bridge design, (PhD Thesis), EPFL, Lausanne, Switzerland, 2008. (285 pp.).